Inorganic remote glass film based on yellowish-green (Y, $Ba)_3(Al, Si)_5O_{12}$:Ce garnet phosphor for warm white LEDs

Yuting Zhang[a], Huan Tu[a], Guoying Zhao*[a], Jingshan Hou[a], Yufeng Liu[a], Xin Qiao[b], Zhongzhi Wang[b], Bo Li[b], Ji-Guang Li[c], Feng Wang*[d], Yongzheng Fang*[a]

* *Corresponding authors*

[a] *School of Materials Science and Engineering, Shanghai Institute of Technology, Shanghai 201418, PR China*

[b] *Baotou Research Institute of Rare Earths, Baotou, 014030, China*

[c] *Research Center for Functional Materials, National Institute for Materials Science, Tsukuba, Ibaraki 305-0044, Japan*

[d] *Department of Materials Science and Engineering, City University of Hong Kong, 83 Tat Chee Avenue, Hong Kong SAR, China*

E-mail addresses: zhaogy135@126.com; fyz1003@sina.com; fwang24@cityu.edu.hk

Abstract: Compared with other fluorescent crystal phases, garnet has better structural stability in a glass matrix and renders precisely controllable emissions due to the abundant lattice control positions. In this work, we regulate the coordination field of Ce_{3+} ion based on the co-substitution method, and achieve the spectra regulation in the yellow-green range. We used Ba^{2+}-Si^{4+} cations to replace Y^{3+}-Al^{3+} cations in $Y_3Al_5O_{12}$ (YAG) matrix to obtain blue-shift of the emission peak from 552 nm to 539 nm. The centroid shift and crystal field splitting decrease with decreasing covalency of the bond between the Ce^{3+} ion and the surrounding anions owing to the higher

electronegativity of Si^{4+} ions than Al^{3+} ions. The corresponding fluorescent films were prepared by a low-temperature co-sintering process based on the as-made Ba^{2+}-Si^{4+} co-substituted phosphor. XRD and SEM images showed that the fluorescence crystals were less eroded and evenly dispersed in the glass matrix. Spectral analysis showed that the garnet phase is protected by using lead-free borosilicate glass with a low melting point, and the quantum efficiency of phosphor-in-glass (PiG) retains 98% of the corresponding phosphor. By adjusting the ratio of garnet phosphor to commercial red nitride phosphors, a warm white fluorescence with a color rendering index of 80.3 and color temperature of 3899 K was obtained. The prepared warm white film has potential application value in the whole spectra field.

Keywords: Garnet structure; Co-substitution strategy; Yellowish-green; Phosphor-in-Glass film.

1. Introduction

As a new generation of lighting devices, white light-emitting diodes (WLEDs) have the advantage of high conversion efficiency. However, typical WLEDs based on $Y_3Al_5O_{12}:Ce^{3+}$ yellow phosphors and blue chips have low color rendering index (Ra< 75) [1-3]. Its color temperature is high due to the deficiency of red light. The packaging method is based on the mixing of phosphor powder and organic epoxy resin. As the operation power and working time increase, the chip temperature can be as high as 150 ~ 200 °C, causing the thermal quenching of the phosphor [4-6]. As a result, several problems have arisen with high-power white light sources, including reduced long-term reliability, reduced luminous performance, and color coordinate shift [7].

In order to overcome the shortcomings of organic packaging materials, phosphor-in-glass (PiG) films were prepared by co-sintering of YAG:Ce phosphor and glass powder to improve the long-term reliability of WLEDs [8-10]. PiG can achieve photochromatic tuning by co-sintering different fluorescent crystal phases at low temperatures, which can be used as a preferred choice in high-power white-light devices [11-13]. PiG film is used to prepare warm white light-emitting devices, which are widely used in signal lamps, indoor and outdoor lighting, etc. [14-17]. Borosilicate glass was selected as the phosphor matrix. Borosilicate glass matrix has obvious advantages over other glass matrices. For example, compared with tellurite, it has excellent sintering properties and high visible light transparency without significant interaction with phosphors [18-20].

In this work, yellow-green phosphors with a garnet structure were prepared by co-ion replacement and integrated into a PiG film by co-sintering at low temperatures. The color rendering quality of warm-white-light devices is improved by making up for blue and yellow depressions [21-23]. We used Ba^{2+}-Si^{4+} cations to replace dodecahedral and tetrahedral sites in the garnet structure. Furthermore, SiO_2-BaO-Al_2O_3-ZnO-Na_2O glass powder was chosen to synthesize YAG-based PiG. We tested the properties of a series of $Y_{2.9-x}(Ba)_xAl_{5-x}Si_xO_{12}$:0.1Ce phosphors, which were mixed with a certain proportion of red nitride phosphors. The structure, luminescence properties, quantum efficiencies, and chromaticity stability of the YAG-based PiG were studied in detail. All the results indicate the as-made prepared YAG-based PiG with excellent thermal stability, easy synthesis, and low cost is a promising candidate

for modular high-brightness solid-state lighting devices.

2. Experimental section

2.1 Materials and Synthesis

The $Y_{2.9-x}(Ba)_xAl_{5-x}Si_xO_{12}$:0.1Ce phosphor was prepared by a high-temperature solid phase method. High-purity raw materials Y_2O_3(99.99%, RHAWN), $BaCO_3$(≥99%, GENERAL-REAGENT), SiO_2(99.99%, Aladdin), Al_2O_3(99.99%, Aladdin), CeO_2(99.99%, Adamas-beta) were selected, and H_3BO_3 was added as a flux. After mixing evenly, the phosphor was prepared by sintering for 6 hours at 1450 ℃ in the reducing atmosphere (5 vol% H_2 and 95 vol% N_2) in the tube furnace. The precursor glass of $28SiO_2$-$39B_2O_3$-$16ZnO$-$17Na_2O$ was fused in a Muffle furnace at 1100 °C for 30 minutes, and then the glass was ground into powders with an agate mortar.

2.2 Fabrication of PiG films

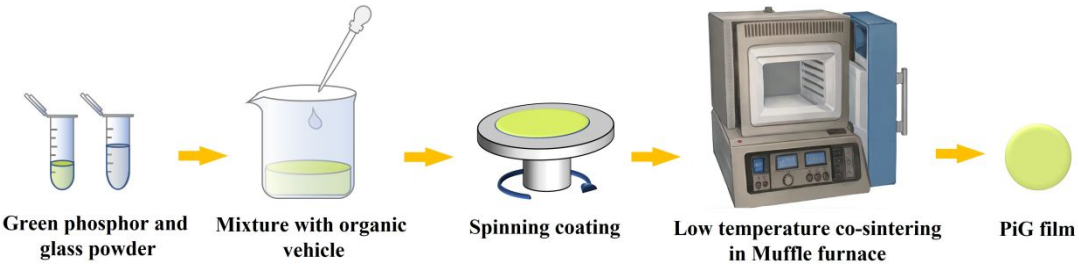

Fig. 1. Fabrication of PiG films by the spin coating technique.

The organic vehicle (terpineol and ethyl cellulose) was evenly mixed at a mass ratio of 10:1 and stirred at 60 °C for 12 hours. Then the organic solvent, phosphor, and glass powder were mixed evenly according to the mass ratio of 2:3:2 to prepare a

non-precipitating, uniform fluorescent slurry. The fluorescent paste is uniformly coated on the quartz glass substrate by a rotating coating method, and then dried for 4 hours in a 150 ℃ electric blast drying oven to fully volatilize the organic matter. Finally, the fluorescent glass film was obtained after secondary co-sintering at 570 ℃ for 20 minutes, which is depicted in Fig. 1.

2.3 Characterizations

The X-ray powder diffractometer (XRD) patterns of phosphor powder and PiG film were determined by X-ray powder diffractometer (TD-3500, Dandong, China). Photoluminescence (PL) and photoluminescence excitation (PLE) spectra were recorded by a Hitachi F-7000 Xenon discharge lamp spectrometer. Field emission scanning microscopy (SEM), and energy dispersive X-ray spectroscopy (EDX) were used to observe the microstructure and element map (Zeiss Gemini 300). The spherical fluorescence spectrometer (SC-30) recorded the quantum efficiency (QE) and the fluorescence spectrometer (FLS920) measured the decay curve. The optical characteristics of the WLEDs, containing electroluminescence, chromaticity coordinate (CIE), correlation color temperature (CCT) and color-rendering index (R_a), were measured in the integrating sphere (HAAS-2000).

3. Result and Discussion

3.1 Microstructure and luminescence of $Y_{2.9-x}(Ba)_xAl_{5-x}Si_xO_{12}$:0.1Ce phosphors

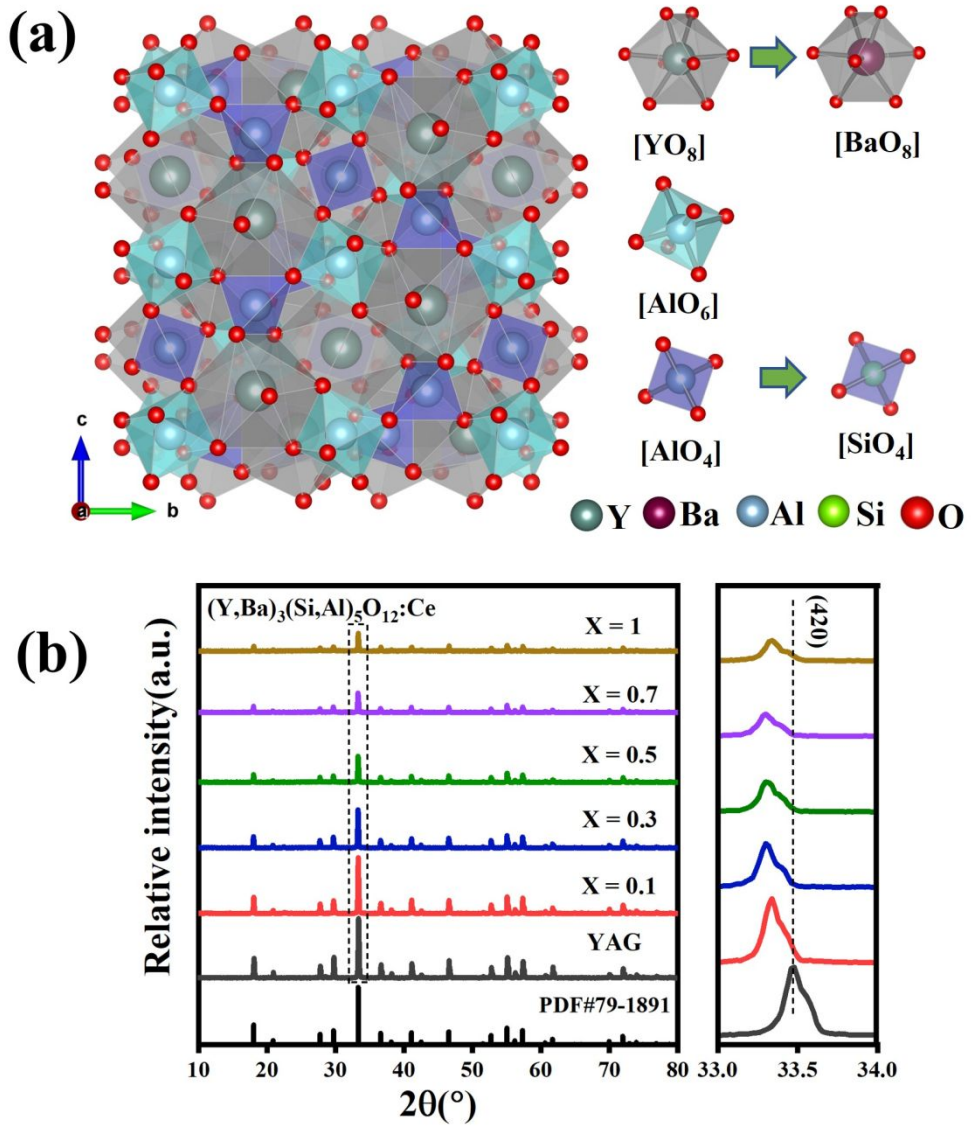

Fig. 2. (a) The crystal structure of $Y_3Al_5O_{12}$ typical unit cell and the substitution of Ba^{2+}-Si^{4+}. (b) XRD patterns of $(Y, Ba)_3(Si, Al)_5O_{12}$:0.1Ce phosphors.

In the garnet YAG-based host, the Ba^{2+}-Si^{4+} substitution involves dodecahedral and tetrahedral. Fig. 2(a) shows the crystal structure of $Y_3Al_5O_{12}$ and the substitution of Ba^{2+}-Si^{4+}. The Ba^{2+} (CN=8, R_{Ba}^{2+}=1.42 Å) and Si^{4+} (CN=6, R_{Si}^{4+}=0.4 Å) ions were

introduced into the typical garnet unit cell, occupying the site of Y^{3+} (CN=8, R_{Y}^{3+}=1.019 Å) and $Al_{(2)}^{3+}$ (CN=4, R_{Al}^{3+}=0.39 Å), respectively. In the octahedral position, the ionic radius of $Al_{(1)}^{3+}$ (CN=4, R_{Al}^{3+}=0.535Å) is much larger than that of Si^{4+} (CN=6, R_{Si}^{4+}=0.4 Å) and Si^{4+} (CN=4, R_{Si}^{4+}=0.26 Å), so Si^{4+} ions cannot replace the octahedral position. The XRD patterns of a series of phosphors were presented in Fig. 2(b). All diffraction peaks can be well indexed with that of standard data of $Y_3Al_5O_{12}$ (PDF#79-1891) without noticeable impurity or secondary phases, indicating the successful incorporation of Ba^{2+}-Si^{4+} in the garnet lattice. In Fig. 2(b), From the magnified XRD pattern in the 33-34°, that the diffraction peaks of the (420) plane presented a gradual shift to the lower angle side range as the Ba2+-Si4+ ratio increases. The lattice expansion due to the substitution of larger Ba^{2+} (CN=8, R_{Ba}^{2+}=1.42 Å) ions for Y^{3+} (CN=8, R_{Y}^{3+}=1.019 Å).

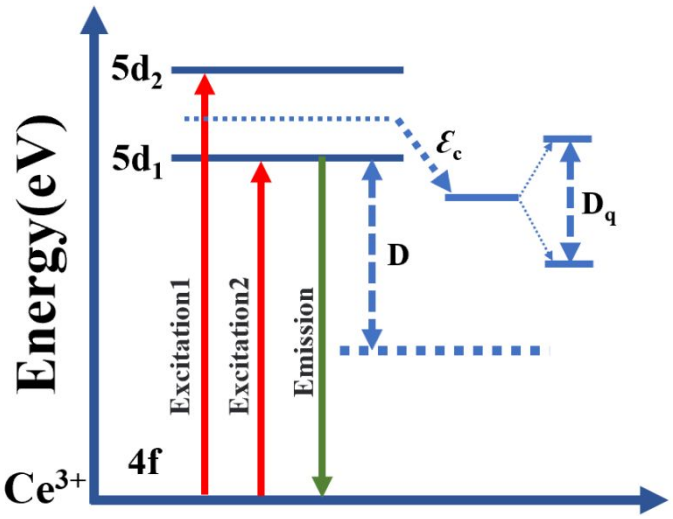

Fig. 3. Schematics of the changes in 5d energy levels of the activator Ce^{3+}.

The interaction of Ce3+ with the ligand significantly affects its luminescence properties. Thus, the chemical environment around Ce3+ is affected with the introduction of Ba2+-Si4+ ions. The energy level structure of Ce3+ is given in Figure

3, which shows the decrease D of the lowest 5d energy level relative to the free ion energy level. The electronegativity of each ion is as follows: Ba^{2+} (EN=0.89), Si^{4+} (EN=1.90), Y^{3+} (EN=1.22), Al^{3+} (EN=1.61), and Ce^{3+} (EN=1.12). Covalency gives rise to a centroid shift ε_c of the degeneracy weighted average 5d energy. The crystal field splitting depends on the bond lengths from the activator ion to the coordinating anions, and the following equation can determine crystal field splitting (D_q): [24-26]

$$D_q = \frac{1}{6} Ze^2 \frac{r^4}{R^5}. \qquad (1)$$

where e is the electron charge, r is the radius of the d wave function, and R is the bond length which mainly affects the field splitting (D_q), Z is the anion charge.

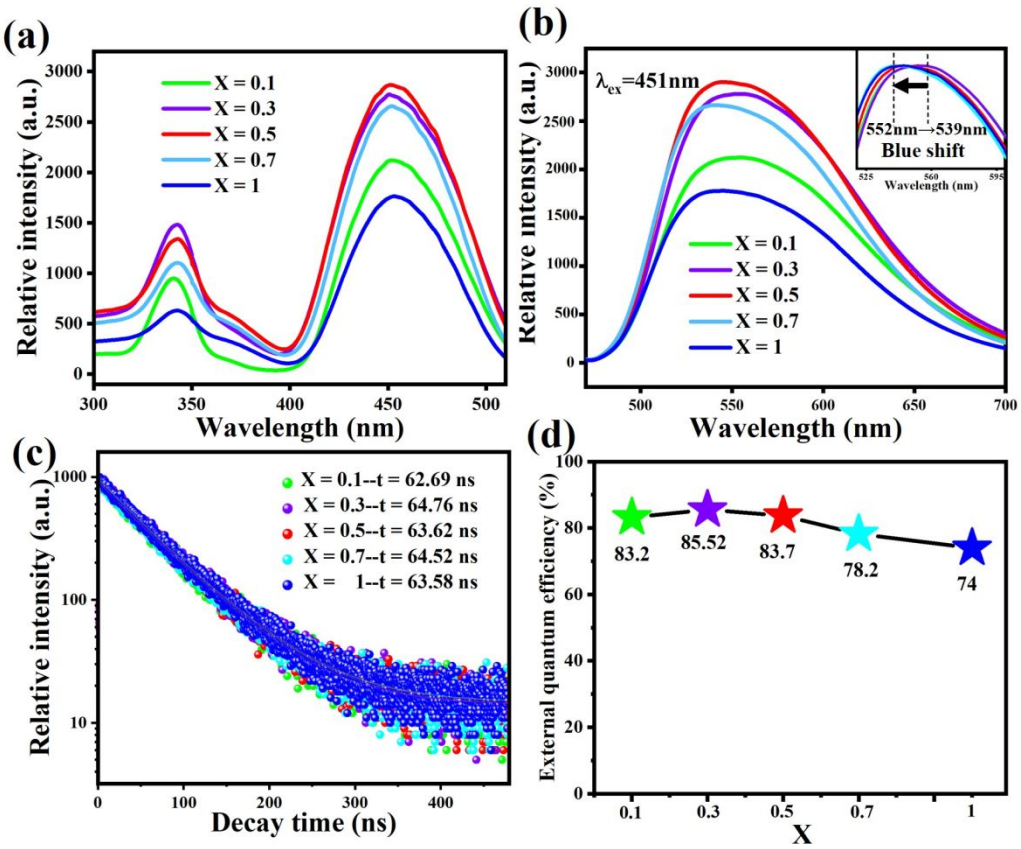

Fig. 4. (a) PLE spectra, (b) PL spectra, (c) luminescence decay curve (detected at 451 nm), and (d) QE of phosphors.

Fig. 4(a-b) depicts the PLE and PL (λ_{ex}=451 nm) of $(Y, Ba)_3(Si, Al)_5O_{12}$:0.1$Ce^{3+}$

phosphor as a function of Ba^{2+}-Si^{4+} content (x values=0.1, 0.3, 0.5, 0.7, 1). In Fig. 4(a), the two excitation bands observed at approximately 340 nm and 450 nm are attributed to electronic transitions of Ce^{3+} from the 4f level to the $5d_2$ and $5d_1$ levels. Fig. 4(b) shows that the emission peak, originating from the $5d_1$ to 4f transition, shifts from 552 nm to 539 nm with the increase of Ba^{2+}-Si^{4+}concentration. In the garnet YAG-based host, the Ba^{2+}-Si^{4+} substitution involves dodecahedral and tetrahedral sites in the garnet structure. This leads to the formation of solid-solution garnets and allows for a continuous variation of the local environment of Ce^{3+}. The ion radius of Ba^{2+} is bigger than that of Y^{3+}, but the radius of Si^{4+} is far smaller than Al^{3+}. Then the bond length (R_{Ce-O}) increased when Si^{4+} ions substituted for the $Al_{(2)}^{3+}$. According to equation (1), the D_q is reduced, shifting the bottom of Ce^{3+} 5d level to higher energy. And at the same time, the electronegativity of Si^{4+} (EN=1.90) is bigger than that of Al^{3+} (EN=1.61) ions, and the ability to attract electrons of Si^{4+} is richer. Thus, with the increase of Si^{4+} ion, the covalence of Ce^{3+} ion and surrounding anions reduces, that is, the centroid shift (ε_c) decreases. In summary, the decrease of crystal field splitting (D_q) and centroid shift (ε_c) leads to the blue-shift of the spectrum.

Fig. 4(c) indicates the luminescence decay curve of the phosphor measured at 451 nm, which were fitted well with the exponential function [27,28]. The introduction of Ba^{2+}-Si^{4+} ions did not significantly change the luminescence lifetime of Ce^{3+} ions [29]. Fig. 4(d) is the quantum efficiency of the sample $Y_{2.9-x}Ba_xAl_{5-x}Si_xO_{12}$:0.1Ce phosphor. When x=0.3, the internal quantum efficiency reaches the maximum value of 85.52%. The internal quantum efficiency of the phosphors with x=0.1, 0.3, and 0.5

are all higher than 80%. It can be seen that the quantum efficiency increases steadily and then gradually decreases. The decrease in quantum efficiency is due to lattice distortion, high solid solubility, and increased lattice disorder. The quantum efficiency of the phosphor sample prepared in this subject is higher than that of $(Y, Ca)_3(Al, Mg)_2(Al, Si)_3O_{12}:Ce^{3+}$ phosphor prepared by Tu and co-workers (78.56%) [30]. The phosphor performance is also superior to that of $(Y, Ca)_3(Al, Si)_5O_{12}:Ce^{3+}$ synthesized under the same conditions (Figs. S1 and S2).

3.2 Microstructure and luminescence of $Y_{2.9-x}(Ba)_xAl_{5-x}Si_xO_{12}$:0.1Ce PiG films

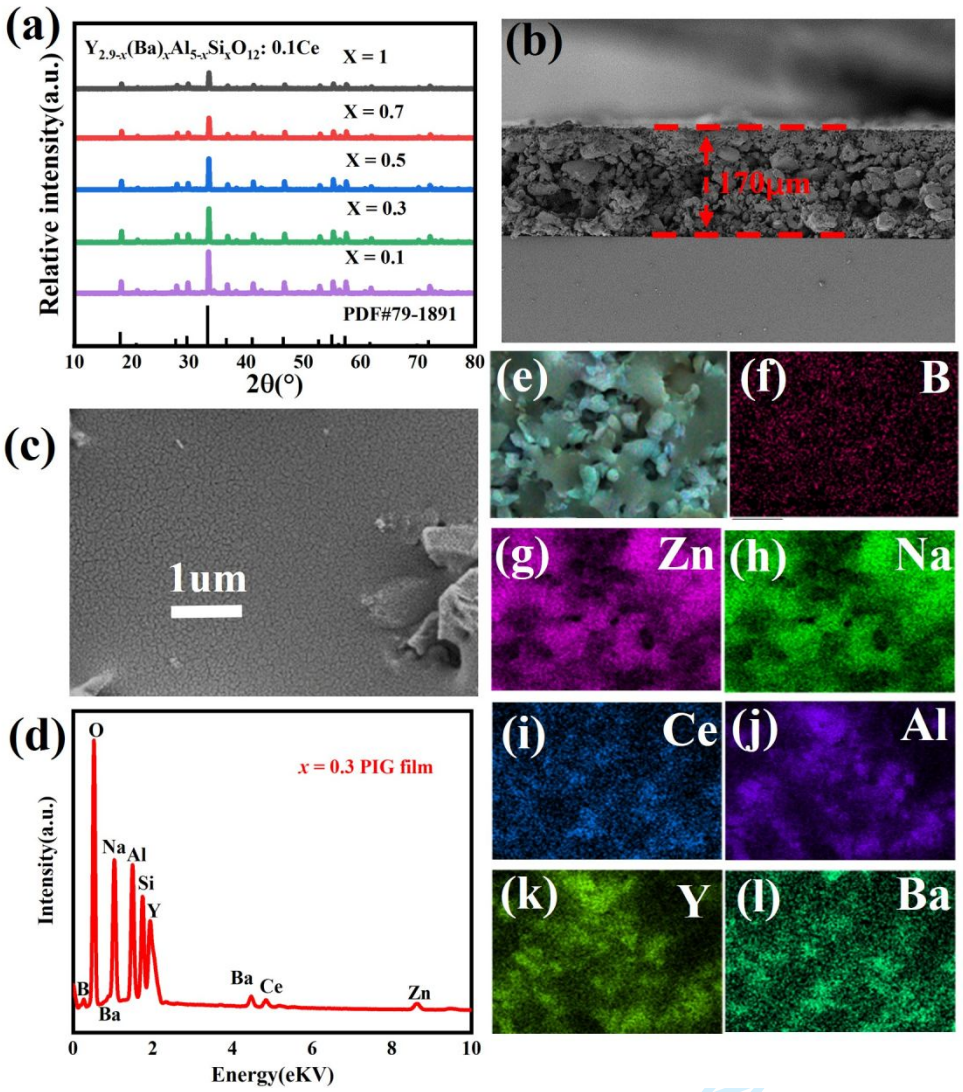

Fig. 5. (a) XRD patterns of PiG thin films. (b) Cross-section image of the film. (c) Top-view SEM image of the film. (d-l) The corresponding EDX spectrum and mapping images.

In Fig. 5(a), the XRD patterns of $Y_{2.9-x}(Ba)_xAl_{5-x}Si_xO_{12}$:0.1Ce PiG films match the standard PDF card No. 79-1891, indicating that the crystallinity of the phosphors was hardly affected during the low-temperature sintering process. Furthermore, PiG film with an x value of 0.3 was selected to explore possible reactions between the glass and the phosphor. Fig. 5(b) shows the cross-sectional image of sample.

Obviously, the phosphor layer adhered well to the surface of the quartz glass substrate after sintering, and a uniform phosphor layer with a thickness of about 170 μm was observed. Moreover, it manifests the microparticles are even-distributed and embedded in the porous glass matrix. The proper pores were beneficial to reducing the reflection of incident light and improve the utilization of light. Fig. 5(c) shows the surface morphology of the film. It can be observed that the surface of the film is uniform, indicating that the phosphor is well distributed in the glass system. There were no detectable intermediate products formed during sintering, as revealed by the EDX spectrum in Fig. 5(d) and elemental maps in Fig. 5(e-l).

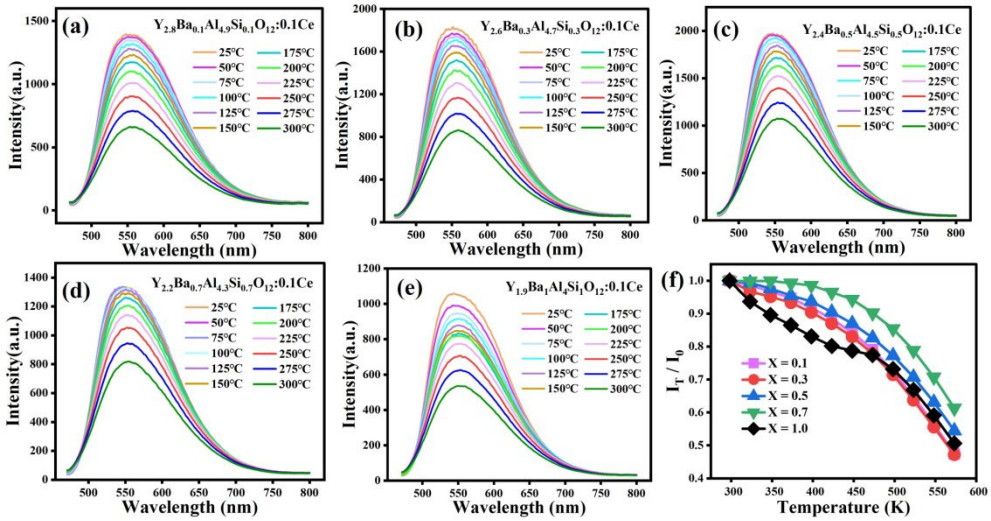

Fig. 6. (a-e) Emission spectral intensity(λ_{ex}=451nm) of $Y_{2.9-x}(Ba)_xAl_{5-x}Si_xO_{12}$:0.1Ce (value x=0.1-1.0) films in the temperature range of 25-300 ℃. (f) Temperature dependent emission intensity at different ion co-substitution concentrations.

Figures 6(a-e) show the temperature-dependent peak emission intensity variation of the films at different concentrations of ion co-substitution， and temperature range of 25-300°C. In Fig. (f), the curve is fitted according to the Arrhenius equation I_T/I_0 =[1+D exp (-E_a/kT)]$^{-1,}$ where I_0 is the intensity at T=25 °C, I_T is the intensity at

different temperatures *T, D* is a constant, Ea is the thermal burst activation energy, and *k* is the Boltzmann constant [31-32]. The highest temperature-dependent emission intensity of the film is up to 85% when the temperature is 500 K. The above shows that the prepared films have excellent thermal stability.

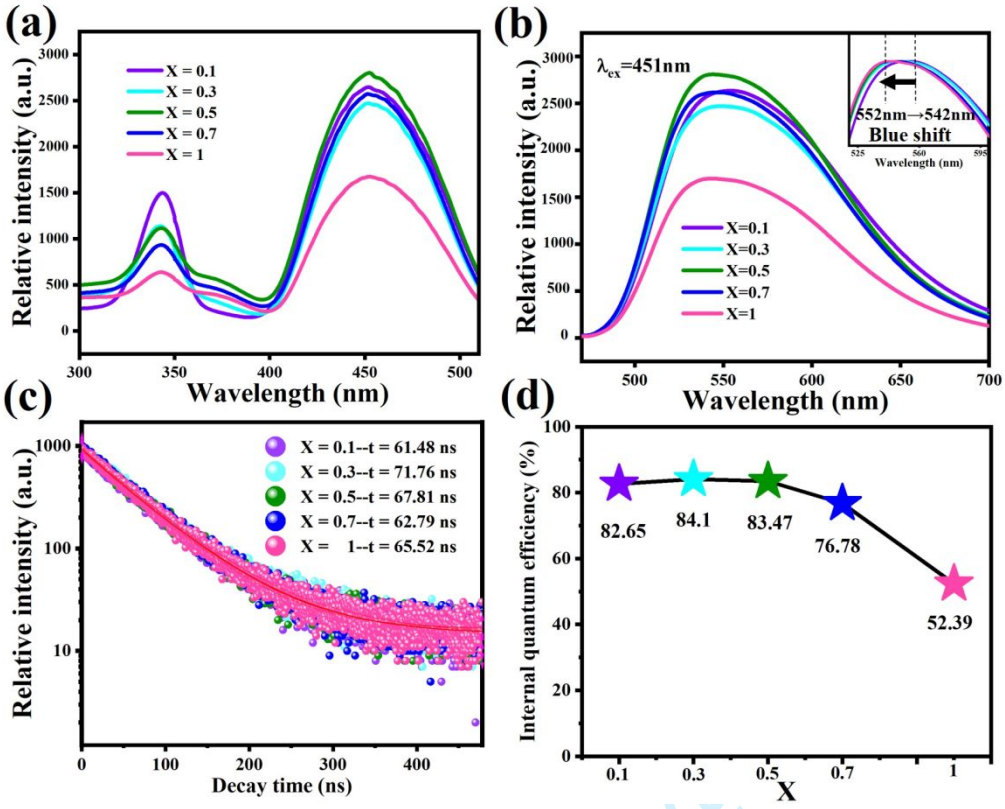

Fig. 7. (a) excitation spectra, (b) emission spectra, (c) decay curves of the PiG films, and (d) QE.

The excitation and emission spectra of $Y_{2.9-x}(Ba)_xAl_{5-x}Si_xO_{12}$:0.1Ce ($0.1 \leq x \leq 1$) PiG films were shown in Fig. 7. In Fig. 7(a), the excitation spectra make up of two broad bands attributed to the $4f \rightarrow 5d_2$ and $4f \rightarrow 5d_1$ electronic transition of Ce^{3+}. In Fig. 7(b), the emission (λ_{ex}=451 nm) peak to the $5d_1 \rightarrow 4f$ transition was observed with a distinct spectrum blue-shift range from 552 nm to 542 nm. The decay curve of films shown in Fig. 7(c) is consistent with the original phosphor. The phosphors maintained

efficient luminescence in the PiG films, demonstrating a high quantum efficiency of 84.1% at x=0.3 (Fig. 7d). At high co-substitution concentrations (i.e., x=1.0), the quantum efficiency decreased significantly. The possible reason is that the glass significantly affects the photons absorption of phosphor in excitation as the concentration of ion co-substitution increases [33]. Therefore, the optimal co-substitution concentration of Ba^{2+}-Si^{4+} into garnet phosphor is around x=0.3.

3.3 Electroluminescence performance of $Y_{2.9-x}(Ba)_xAl_{5-x}Si_xO_{12}$:0.1Ce PiG films

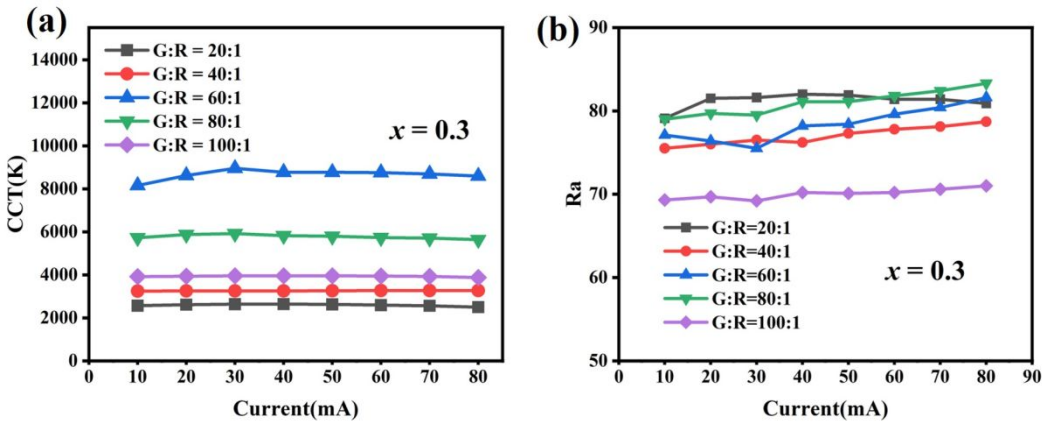

Fig. 8. (a) Color temperature and (b) color render index of the PiG films composed of $Y_{2.9-x}(Ba)_xAl_{5-x}Si_xO_{12}$:0.1Ce ($x$=0.3) and red nitride phosphor at the ratios of 100:1, 80:1, 60:1, 40:1, and 20:1 respectively.

Table 1

Comparison of CCT and Ra among different phosphors.

Group	Phosphor	CCT(K)	Ra	Ref.
1	$Y_{2.74}Ca_{0.2}Al_{1.6}M_{0.4}Al_{2.4}Si_{0.6}O_{12}$:0.06$Ce^{3+}$	4858	74.4	[30]
2	5 wt% of commercial $Y_3Al_5O_{12}$:Ce^{3+}	3700-4200	60	[34]
3	YAG:Ce polycrystalline ceramics with	5351	75.9	[35]

	different SiO_2			
4	$La_2LiTaO_6:Mn^{4+}$	5500	72	[36]
5	$Y_{2.6}Ba_{0.3}Al_{4.7}Si_{0.3}O_{12}:0.1Ce^{3+}$	<4000	80.3	This work

The photoluminescence properties of PiG films can be adjusted by adding heterogeneous phosphors. The green phosphors obtained in this study lacked red light, so a certain proportion of commercial red nitride phosphors should be added to prepare polychromatic fluorescent films. The ratio of green powder to red powder (GtR) was 100:1, 80:1, 60:1, 40:1, and 20:1, respectively. The relevant color temperature and color rendering indexes are shown in Fig. 8(a) and (b), respectively. At the ratios of 100:1, 40:1, and 20:1, the color temperature of these three samples is lower than 4000 K. Meanwhile, high color rendering indices of 83.3, 81.6, and 82 were achieved at the ratios of 80:1, 60:1, and 20:1. These results provide an idea for the preparation of the color converter of warm white devices with low color temperature and high color rendering index. For comparison, the color temperature and color rendering index reported in other works are compiled in Table 1 [30,34-36]. It can be seen that this sample has a significant advantage of low color temperature and high color rendering index, which can effectively compensate for the yellow-blue depression and can be used to prepare high-quality warm white color converters.

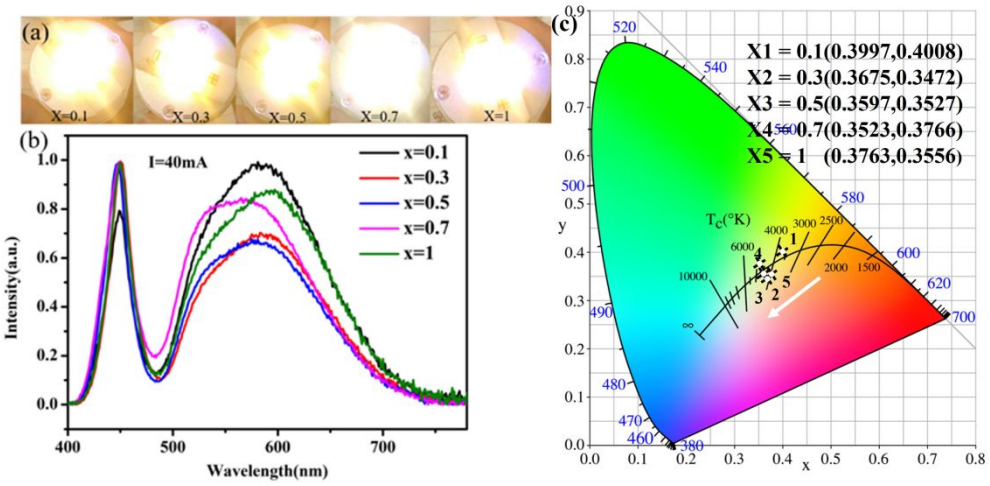

Fig. 9. (a) Photographs, (b) electroluminescence spectra, and (c) CIE chromaticity coordinates of the PiG films of $Y_{2.9-x}(Ba)_xAl_{5-x}Si_xO_{12}$:0.1Ce ($0.1 \leq x \leq 1$) with a red to green phosphor (GtR) ratio of 80:1.

In a further set of experiments, the PiG films were encapsulated with commercial blue chips for warm white light emission (Fig. S3). Fig. 9(a) shows the luminescence performance test of $Y_{2.9-x}(Ba)_xAl_{5-x}Si_xO_{12}$:0.1Ce ($0.1 \leq x \leq 1$) PiG films with GtR of 80:1 at 40 mA. The corresponding electroluminescence spectra are shown in Fig. 9(b). The broad emission band centered at about 570 nm is assigned to Ce^{3+}:$5d_1 \rightarrow 4f$ transition under excitation of 450 nm. In Fig. 9(c), the CIE chromaticity coordinate of PiG-based white WLEDs locates at the warm white light region, which shifts from yellowish-green to yellowish-white, in consistency with their actual illumination photographs in Fig. 9(a). The substitution of Y^{3+}-Al^{3+} ions by larger Ba^{2+}-Si^{4+} ions in garnet crystal provides a feasibility strategy for chromaticity-tunable remote WLEDs.

4. Conclusion

In the work of this subject, $Y_{2.9-x}(Ba)_xAl5_{-x}Si_xO12$:0.1Ce phosphors were prepared by a high-temperature solid-phase method. The blue shift of emission

spectra is realized from 552 nm to 539 nm, with an optimum quantum efficiency of 85.52%. We further obtained fluorescent glass films by spin coating and post sintering. The PiG maintained a high quantum efficiency of 84.1%, and the emission profile can be fine-tuned by the inclusion of a secondary phosphor of borosilicate glass at precisely controlled ratios. By using the PiG engineering strategy, we demonstrated a robust light converter that can be used to prepare high-quality warm white light with a blue LED chip.

Acknowledgement

Yongzheng Fang acknowledges financial support from the National Key Research and Development Program (No. 2021YFB3500500) and the National Natural Science Foundation of China (No. 51472162). Guoying Zhao acknowledges financial support from Science and Technology Talents Development Fund for Young Middle-aged Teachers Fund, Collaborative Innovation Fund (No. XTCX2022-03) of Shanghai Institute of Technology and Development of key technologies for the preparation and application of high-performance rare earth fluorescent block materials (No. BFXT-2022-D0046). Jingshan Hou acknowledges financial support from the National Natural Science Foundation of China (No. 51902203).

REFERENCES

[1] C.C. Lin, R.S. Liu, Advances in phosphors for light-emitting diodes, J. Phys. Chem. Lett. 2 (2011) 1268-1277.

[2] S. Ye, F. Xiao, Y.X. Pan, Y.Y. Ma, Q.Y. Zhang, Phosphors in phosphor-converted white light-emitting diodes: Recent advances in materials, techniques and properties, Mat. Sci. Eng. R. 71 (2010) 1-34.

[3] B. Wang, Y.G. Liu, Z. Huang, M. Fang, X. Wu, Discovery of novel solid solution $Ca_3Si_{3-x}O_{3+x}N_{4-2x}$: Eu^{2+} phosphors: structural evolution and photoluminescence tuning, Sci. Rep. 7 (2017) 18103.

[4] J. Deng, W. Li, H. Zhang, Y. Liu, B. Lei, H. Zhang, L. Liu, X. Bai, H. Luo, H. Liu, W.R. Liu, J. Wang, Eu^{3+}-Doped Phosphor-in-Glass: A Route toward Tunable Multicolor Materials for Near-UV High-Power Warm-White LEDs, Advanced Optical Materials. 5 (2017) 1600910.

[5] H. Chen, H. Lin, J. Xu, B. Wang, Z. Lin, J. Zhou, Y. Wang, Chromaticity-tunable phosphor-in-glass for long-lifetime high-power warm w-LEDs, J. Mater. Chem. C. 3 (2015) 8080-8089.

[6] D. Chen, S. yuan, X. Li, W Xu, Dual-phase phosphor-in-glass based on a Sn-P-F-O ultralow-melting glass for warm white light-emitting diodes, RSC advances. 7 (2017) 36168-36174.

[7] H. Zhu, C.C. Lin, W. Luo, S. Shu, Z. Liu, Y. Liu, J. Kong, E. Ma, Y. Cao, R.S. Liu, X. Chen, Highly efficient non-rare-earth red emitting phosphor for warm white light-emitting diodes, Nat. Commun. 5 (2014) 4312−4321.

[8] S.C. Allen, A.J. Steckl, A nearly ideal phosphor-converted white light-emitting diode, Appl. Phys. Lett. 92 (2008) 143309.

[9] L. Yang, M. Chen, Z. Lv, S. Wang, X. Liu, S. Liu, Preparation of a YAG: Ce phosphor glass by screen-printing technology and its application in LED packaging, Opt. Lett. 38 (2013) 2240–2243.

[10] F. Wang, Y. Lin, H. Shi, W. Wang, Z. Deng, J. Chen, X. Yuan, Y. Cao,

Introduction on the fabrication technique of phosphor in glass by tape-casting and investigation on the chromaticity property, Opt. Express. 22 (2014) A1355–A1362.

[11] E. Kim, S. Unithrattil, I.S. Sohn, S.J. Kim, W.J. Chung, W.B. Im, Facile one-step fabrication of 2-layered and 4-quadrant type phosphor-in-glass plates for white LEDs: an insight into angle dependent luminescence, Opt. Mater. Express. 6 (2016) 804−814.

[12] D. Chen, W. Xiang, X. Liang, J. Zhong, H. Yu, M. Ding, H. Lu, Z. Ji, Advances in transparent glass–ceramic phosphors for white light-emitting diodes—A review, J. Eur. Ceram. Soc. 35 (2015) 859−869.

[13] R. Zhang, H. Lin, Y. Yu, D. Chen, J. Xu, Y. Wang, A new-generation color converter for high-power white LED: transparent Ce^{3+}: YAG phosphor-in-glass, Laser & Photonics Rev. 8 (2014) 158−164.

[14] L. Wang, R.J. Xie, T. Suehiro, T. Takeda, N. Hirosaki, Down-Conversion Nitride Materials for Solid State Lighting: Recent Advances and Perspectives, Chemical reviews. 118 (2018) 1951-2009.

[15] S Pimputkar, J.S Speck, S.P DenBaars, S Nakamura, Prospects for LED lighting, Nature photonics. 3 (2009) 180-182.

[16] X. Huang, Red phosphor converts white LEDs, Nature Photonics. 8 (2014) 748-749.

[17] E.F. Schubert, J.K. Kim, Solid-State Light Sources Getting Smart, Science. 308 (2005) 1274-1278.

[18] M.L. Öveçoğlu, G. Özen, S. Cenk, Micro-structural characterization and

crystallization behavior of (1 − x) $TeO_{2-x}WO_3$ (x = 0.15, 0.25, 0.3 mol) glasses, J. Eur. Ceram Soc. 26 (2006) 1149–58.

[19] B. Öz, I. Kabalc, M.L. Öveçoğlu, G. Özen, Thermal properties and crystallization behavior of some TeO_2–K_2O glasses, J. Eur. Ceram. Soc. 27 (2007) 1823–7.

[20] Y.K. Lee, J.S. Lee, J. Heo, W.B. Im, W.J. Chung. Phosphor in glasses with Pb-free silicate glass powders as robust color-converting materials for white LED applications, Opt Lett. 37 (2012) 3276–8.

[21] N.C. George, K.A. Denault, R. Seshadri, Phosphors for solid-state white lighting, Annu. Rev. Mater. Res. 43 (2013) 481–501.

[22] H.T. Kim, J.H. Kim, J.K. Lee, C.K. Yun, Green light-emitting $Lu_3Al_5O_{12}$: Ce phosphor powders prepared by spray pyrolysis, Mater. Res. Bull. 47 (2012) 1428–1431.

[23] J.S. Lee, P. Arunkumar, S. Kim, I.J. Lee, H. Lee, W.B. Im, Smart design to resolve spectral overlapping of phosphor-in-glass for high-powered remote-type white light-emitting devices, Opt. Lett. 39 (2014) 762–765.

[24] Y.H. Kim, H.J. Kim, S.P. Ong, Z. Wang, W.B. Im, Cation-Size Mismatch as a Design Principle for Enhancing the Efficiency of Garnet Phosphors, Chem. Mater. 32, 3097-3108(2020)

[25] L. Zhang, S. Chen, S. Zhao, J. Guo, Q. Lv, H. Wang, B. Deng, G. Zhang, R. Yu, H. Geng, Thermal stability and luminescence of novel garnet-type yafsoanite $Ca_3Zn_3(TeO_6)_2$: Sm^{3+} phosphors for white LEDs, Ceram. Int. 47 (2021) 11887-11898.

[26] M. Shang, J. Fan, H. Lian, Y. Zhang, D. Geng, J. Lin, A Double Substitution of Mg^{2+}-Si^{4+}/Ge^{4+} for $Al_{(1)}^{3+}$-$Al_{(2)}^{3+}$ in Ce^{3+}-Doped Garnet Phosphor for White LEDs, Inorg. Chem. 53 (2014) 7748-7755.

[27] F. Lahoz, I.R. Martín, J. Méndez-Ramos, Dopant distribution in a Tm^{3+}-Yb^{3+} codoped silica-based glass ceramic: An infrared-laser induced up conversion study, J. Chem. Phys. 120 (2004) 6180–6190.

[28] Q.H. Meng, X.J. Wang, Q. Zhu, J.G. Li, The effects of Mg^{2+}/Si^{4+} co-substitution for Al^{3+} on sintering and photoluminescence of $(Gd, Lu)_3Al_5O_{12}$: Ce garnet ceramics, J. Eur. Ceram. Soc. 40 (2020) 3262–3269.

[29] X. Li, L. Wang, Q.Q. Zhu, D.M. Tang, X.J. Liu, G.F. Cheng, L. Lu, T. Takeda, N. Hirosaki, Z.R. Huang, R.-J. Xie, Crystal Structure, Tunable Emission and Applications of $Ca_{1-x}Al_{1-x}Si_{1+x}N_{3-x}O_x$: RE (x=0-0.22, RE=$Ce^{3+}$, Eu^{2+}) Solid Solution Phosphors for White Light-Emitting Diodes, J. Mater. Chem. C 4 (2016) 11219−11230.

[30] H. Tu, G.Y. Zhao, J.S. Hou, Y.F. Liu, Y. Zhou, G. H. Zhang, H.T. Sun, J.G. Li, Y.Z. Fang, A garnet-structured $(Y, Ca)_3(Al, Mg)_2(Al, Si)_3O_{12}$: Ce^{3+} phosphor-in-glass engineering for use in high color rendering white LEDs, AIP Advances. 12 (2022) 055113.

[31] X. Wang, T. Seto, Z. Zhao, Y. Li, Q. Wu, H. Li, Y. Wang, Preparation of $Sr_{1-x}Ca_xYSi_4N_7$:Eu^{2+} solid solutions and their luminescence properties, Journal of Materials Chemistry C, 2 (2014) 4476.

[32] S.X. Li, L. Wang, Q.Q. Zhu, D.M. X.J. Tang, G.F. Cheng, L. Lu, T. Takeda, N.

Hirosaki, Z.R. Huang, R. J. Xie, Crystal structure, tunable emission and applications of $Ca_{1-x}Al_{1-x}Si_{1+x}N_{3-x}O_x$:RE (x= 0–0.22, RE= Ce $^{3+}$, Eu $^{2+}$) solid solution phosphors for white light-emitting diodes, Journal of Materials Chemistry C, 4 (2016) 11219-11230.

[33] G. Liu, Z.F. Tian, Z.H. Chen, H.Z. Wang, Q.H. Zhang, Y.G. Li, CaAlSiN3: Eu^{2+} phosphors bonding with bismuth borate glass for high power light excitation, Optical Materials. 40 (2015): 63-67.

[34] Y. Kim, S. Kim, F. Iqbal, H. Yie, H Kim, Effect of transmittance on luminescence properties of phosphor-in-glass for LED packaging, Optics express. 23 (2015) A43-A50.

[35] M. Gong, W Xiang, J. Huang, C. Yin, X. Liang, Facile synthesis and optical properties of Ce: YAG polycrystalline ceramics with different SiO_2 content, RSC advances. 5 (2015) 75781-75786.

[36] L. Wang, L. Yuan, Y. D. Xu, R. L. Zhou, B. Y. Qu, N. Ding, M. Shi, B. Zhang, Y. Q. Chen, Y. Jiang, D. Wang and J. Y. Shi, Luminescent properties of La_2LiTaO_6: Mn^{4+} and its application as red emission LEDs phosphor, Appl. Phys. A. 117 (2014) 1777–1783.

Supplementary Information

Inorganic remote glass film based on yellowish-green (Y, Ba, Ca)$_3$(Al, Si)$_5$O$_{12}$: Ce garnet phosphor for warm white LEDs.

Yuting Zhang[a], Huan Tu[a], Guoying Zhao*[a], Jingshan Hou[a], Yufeng Liu[a], Xin Qiao[b], Zhongzhi Wang[b], Bo Li[b], Ji-Guang Li[c], Feng Wang*[d], Yongzheng Fang*[a]

* *Corresponding authors*

[a] *School of Materials Science and Engineering, Shanghai Institute of Technology, Shanghai 201418, PR China*

[b] *Baotou Research Institute of Rare Earths, Baotou, 014030, China*

[c] *Research Center for Functional Materials, National Institute for Materials Science, Tsukuba, Ibaraki 305-0044, Japan*

[d] *Department of Materials Science and Engineering, City University of Hong Kong, 83 Tat Chee Avenue, Hong Kong SAR, China*

E-mail addresses: zhaogy135@126.com; fyz1003@sina.com; fwang24@cityu.edu.hk

The fluorescence decay curve was fitted with the following exponential function:

$$I_t = I_0 + A_1 e^{(-t/\tau)} + A_2 e^{(-t/\tau)}$$

where I_t is the luminous intensity at time t, I_0 is constant and τ is the radiative decay time, A_1 and A_2 are decay constants. The following function can be used to calculate the fluorescence decay time (τ_{exp}):

$$\tau_{exp} = (A_1\tau_1^2 + A_1\tau_1^2)/(A_1\tau_1 + A_2\tau_2)$$

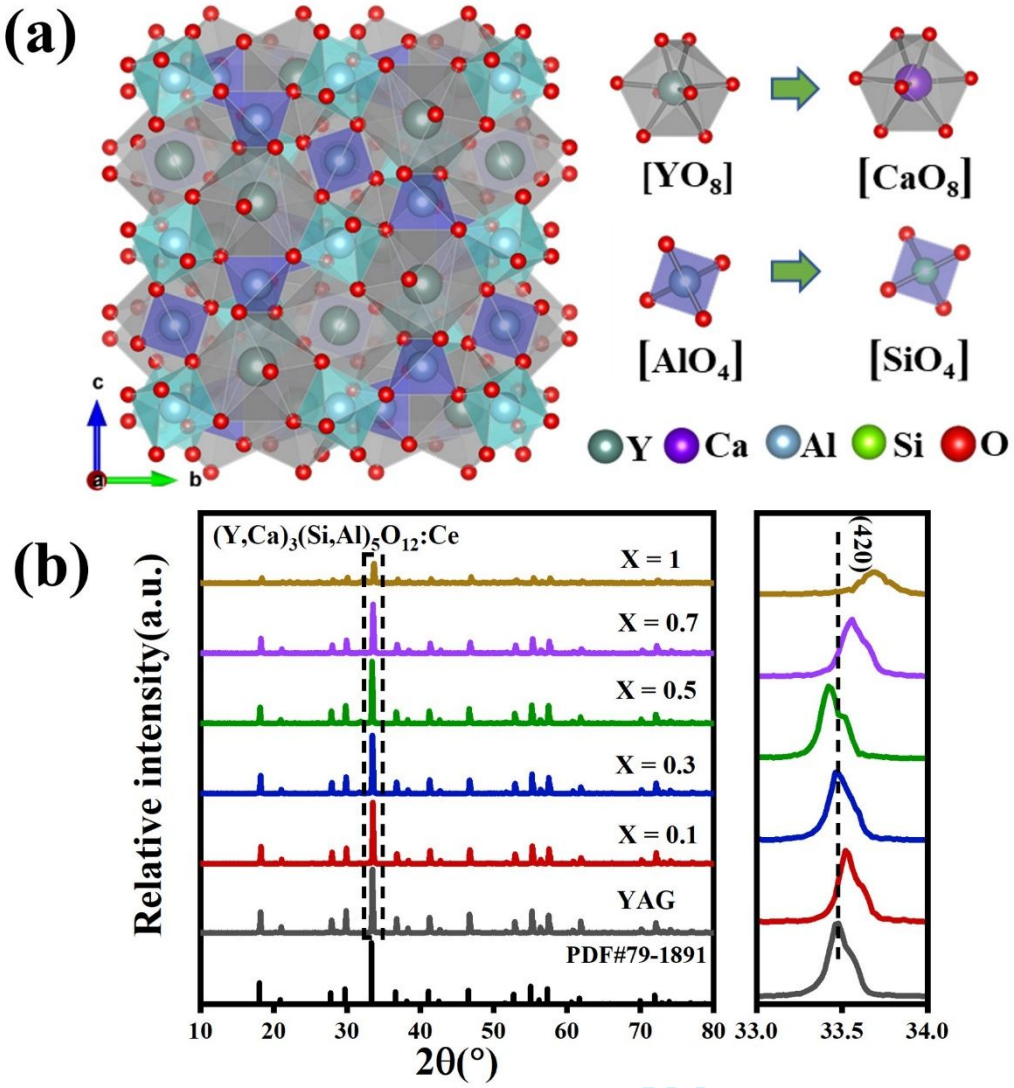

Fig. S1. (a) The crystal structure of $Y_3Al_5O_{12}$ typical unit cell and the substitution of Ca^{2+}-Si^{4+}. (b) XRD patterns of (Y, Ca)$_3$(Si, Al)$_5O_{12}$: 0.1Ce phosphors.

Fig. S1(a) shows the crystal structure of $Y_3Al_5O_{12}$ and the substitution of Ca^{2+}-Si^{4+}. The Ca^{2+} (CN=8, R_{Ca}^{2+}=1.12 Å), Si^{4+} (CN=6, R_{Si}^{4+}=0.4 Å) ions were introduced into the typical garnet unit cell, which occupy the site of Y^{3+} (CN=8, R_Y^{3+}=1.019 Å) and $Al_{(2)}^{3+}$ (CN=4, R_{Al}^{3+}=0.39 Å), respectively. The XRD patterns of a series of phosphors are presented in Fig. 2(b). All diffraction peaks can be well indexed with that of standard data of $Y_3Al_5O_{12}$ (JCPDS No.79-1891) without noticeable impurity or secondary

phases. Fig. S2(b) shows that the diffraction peaks of the (420) plane displayed a gradual shift to the higher angle from the magnified XRD pattern in the 33-34° range as the Ca^{2+}-Si^{4+} ratio increases. The results are ascribed to the smaller ionic radii of Si^{4+} (CN=4, R_{Si}^{4+}=0.26 Å) and Si4+ (CN=6, R_{Si}^{4+}=0.4 Å) than those of $Al(1)^{3+}$ (CN=4, R_{Al}^{3+}=0.535 Å) and $Al(2)^{3+}$ (CN=4, R_{Al}^{3+}=0.39 Å), leading to polycondensation of the crystal lattice.

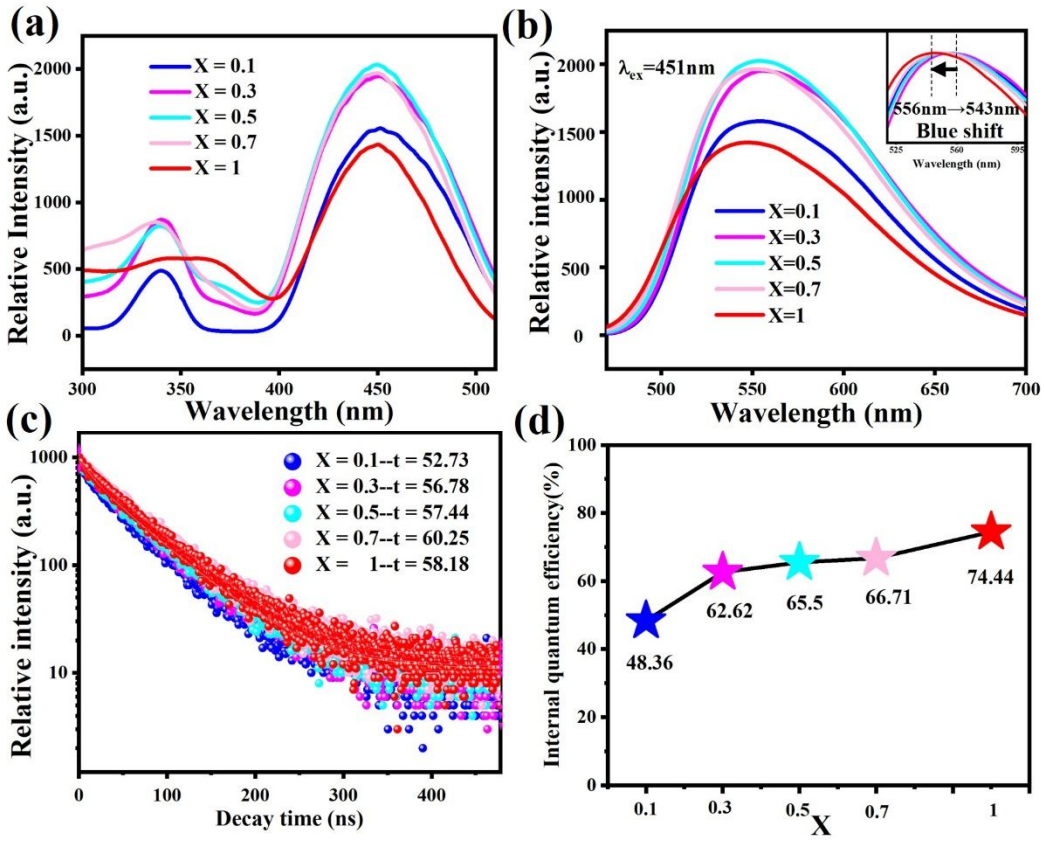

Fig. S2. (a) PLE spectra, (b) PL spectra, (c)luminescence decay curve (detected at 451 nm), and (d) QE of the as-prepared phosphors.

As a control experiment, ion co-substitution of Ca^{2+}-Si^{4+} was studied, demonstrating a spectrum blue shift from 556 nm to 543 nm (Fig. S2). Compared with Ba^{2+}-Si^{4+}, the decay time is reduced by 6.8 ns on average, and the highest quantum efficiency is 74.44%. Therefore, Ba^{2+}-Si^{4+} co-substituted solid solution phosphors are

superior to the co-substitution of Ca^{2+}-Si^{4+} in terms of fluorescence decay time and quantum efficiency.

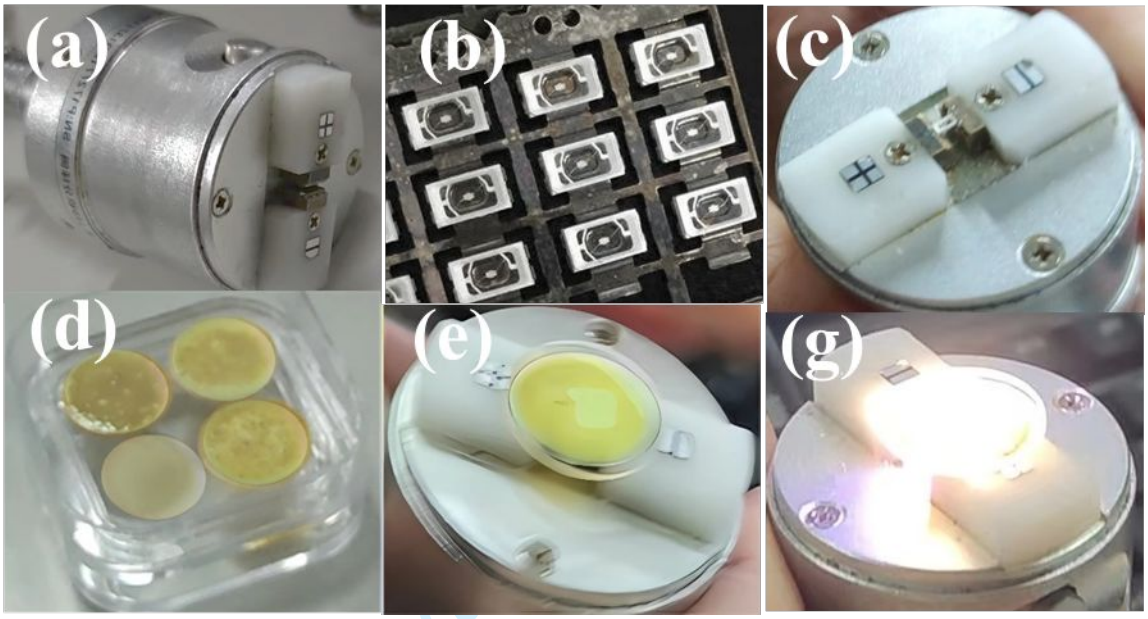

Fig. S3. WLED device fabrication process. (a) The LED capsulation jig. (b) blue LED chip. (c) The LED capsulation jig accompanied with blue LED chip. (d) PiG films. (e) WLED encapsulated by PiG film. (g) PiG film based WLED in operation.

Graphical abstract Image

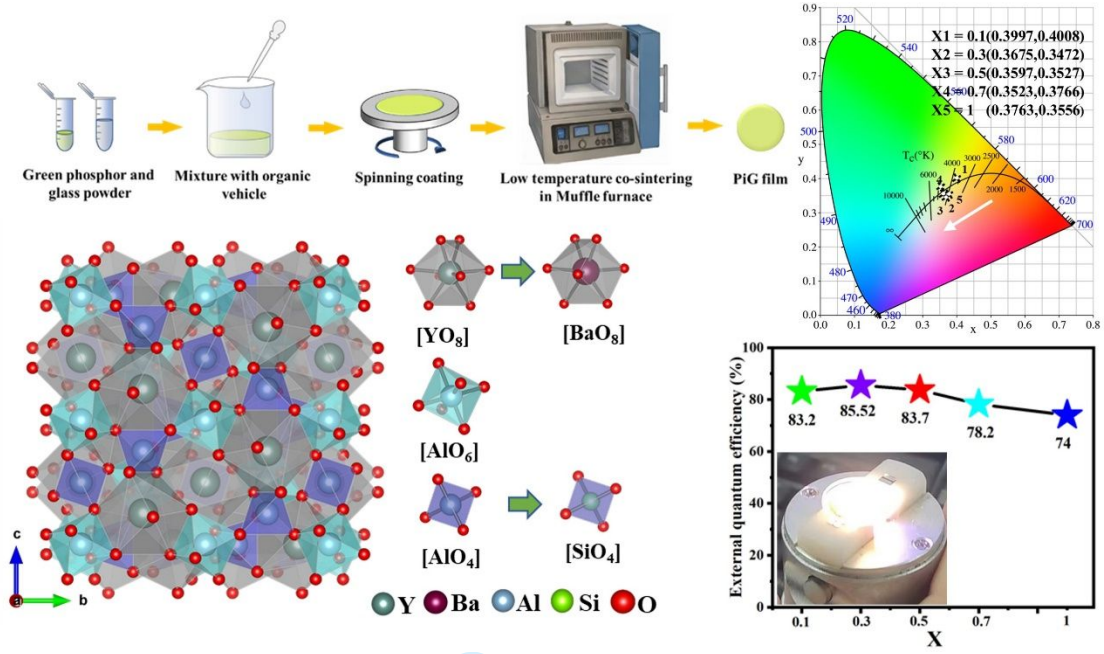

Brief Summary

By used Ba^{2+}-Si^{4+} cations to replace Y^{3+}-Al^{3+} cations in $Y_3Al_5O_{12}$ matrix to obtain yellowish-green phosphor with a quantum efficiency of 85.52%. The corresponding fluorescent films were prepared with a color rendering index of 80.3 color and temperature of 3899 K.